The EMBO Journal Vol. 19 No. 10 pp. 2270–2279, 2000

Structural basis of the Axin–adenomatous polyposis coli interaction

Katharine Eklof Spink, Paul Polakis[1,2] and William I.Weis[3]

Department of Structural Biology, Stanford University School of Medicine, 299 Campus Drive West, Stanford, CA 94305 and [1]Onyx Pharmaceuticals, 3031 Research Drive, Richmond, CA 94806, USA

[2]Present address: Genentech, Inc., 1 DNA Way, MS #40, South San Francisco, CA 94080, USA

[3]Corresponding author
e-mail: bill.weis@stanford.edu

Axin and the adenomatous polyposis coli (APC) tumor suppressor protein are components of the Wnt/Wingless growth factor signaling pathway. In the absence of Wnt signal, Axin and APC regulate cytoplasmic levels of the proto-oncogene β-catenin through the formation of a large complex containing these three proteins, glycogen synthase kinase 3β (GSK3β) and several other proteins. Both Axin and APC are known to be critical for β-catenin regulation, and truncations in APC that eliminate the Axin-binding site result in human cancers. A protease-resistant domain of Axin that contains the APC-binding site is a member of the regulators of G-protein signaling (RGS) superfamily. The crystal structures of this domain alone and in complex with an Axin-binding sequence from APC reveal that the Axin–APC interaction occurs at a conserved groove on a face of the protein that is distinct from the G-protein interface of classical RGS proteins. The molecular interactions observed in the Axin–APC complex provide a rationale for the evolutionary conservation seen in both proteins.

Keywords: Axin/adenomatous polyposis coli/crystal structure/regulators of G-protein signaling/Wnt signaling

Introduction

The Wnt growth-factor signaling pathway plays an essential role in the development of diverse organisms including *Dictyostelium*, *Drosophila*, *Xenopus* and humans (Ginsburg and Kimmel, 1997; Dale, 1998). Although the details of the pathway appear to differ among organisms, the final result of a Wnt signal is an alteration of transcriptional regulation by stabilization of the protein β-catenin. Targets of such regulation include the segment polarity genes *engrailed* and *ultrabithorax* in *Drosophila* (Riese *et al*., 1997; van de Wetering *et al*., 1997), and axis induction genes *siamois* and *Xnr-3* in *Xenopus* (Brannon *et al*., 1997; Fan *et al*., 1998).

Inappropriate activation of Wnt signaling by mutation of pathway components has been observed in a vast number of human cancers including colon carcinomas (Miyoshi *et al*., 1992; Ilyas *et al*., 1997; Morin *et al*., 1997), melanoma (Rubinfeld *et al*., 1997b), medulloblastoma (Zurawel *et al*., 1998), hepatocellular carcinomas (Miyoshi *et al*., 1998) and ovarian (Palacios and Gamallo, 1998) and uterine (Fukuchi *et al*., 1998) cancers (Polakis, 1999). Wnt and β-catenin, both positive effectors of the pathway, have been identified as proto-oncogenes and the adenomatous polyposis coli (APC) protein, a negative regulator, functions as a tumor suppressor (Dale, 1998; Willert and Nusse, 1998; Polakis, 1999). Recent studies suggest that Axin, another negative regulator of the pathway, may also function as a tumor suppressor (Satoh *et al*., 2000). The role of the Wnt pathway in human cancers has been further demonstrated by the identification of the proto-oncogenes c-*MYC*, *cyclin D1* and *WISP-1* as targets of Wnt-mediated transcription in humans (He *et al*., 1998; Shtutman *et al*., 1999; Tetsu and McCormick, 1999; Xu *et al*., 2000).

In the absence of a Wnt signal, glycogen synthase kinase-3β (GSK3β) targets β-catenin for ubiquitin-mediated degradation by phosphorylation of conserved N-terminal serine and threonine residues (Orford *et al*., 1997). GSK3β-mediated phosphorylation of β-catenin requires the formation of a large, multiprotein complex containing GSK3β, β-catenin, APC and Axin. β-catenin, APC and Axin interact with one another. A series of three 15 amino acid and seven 20 amino acid repeats near the center of the APC sequence appears to mediate the APC–β-catenin interaction (Figure 1A) (Su *et al*., 1993; Rubinfeld *et al*., 1996, 1997a). Expression of wild-type APC in cancer cell lines results in a pronounced reduction of cytoplasmic β-catenin levels (Munemitsu *et al*., 1995). However, the role of APC in targeting β-catenin for phosphorylation and degradation is poorly understood.

Axin, named for its role in axis inhibition in vertebrates (Zeng *et al*., 1997), is a negative regulator of the Wnt signaling pathway, as its overexpression results in β-catenin down-regulation (Hart *et al*., 1998). Axin and the related protein axil/conductin contain separate binding sites for β-catenin, GSK3β and APC (Behrens *et al*., 1998; Ikeda *et al*., 1998; Kishida *et al*., 1998; Sakanaka *et al*., 1998; Yamamoto *et al*., 1998) (Figure 1B). Moreover, Axin is the only member of the ternary APC–Axin–β-catenin complex that appears to have direct GSK3β-binding activity (Hart *et al*., 1998). *In vitro* phosphorylation of β-catenin by GSK3β fails in the absence of Axin (Rubinfeld *et al*., 1996), but the addition of Axin promotes phosphorylation in a dose-dependent manner (Ikeda *et al*., 1998). Recently, Axin has also been shown to homodimerize, and to bind to several other proteins involved in Wnt signaling, including protein phosphatase 2A (PP2A) and Dishevelled (Fagotto *et al*., 1999; Hsu *et al*., 1999; Sakanaka and Williams, 1999; Smalley *et al*., 1999) (Figure 1B). Hence, it appears that

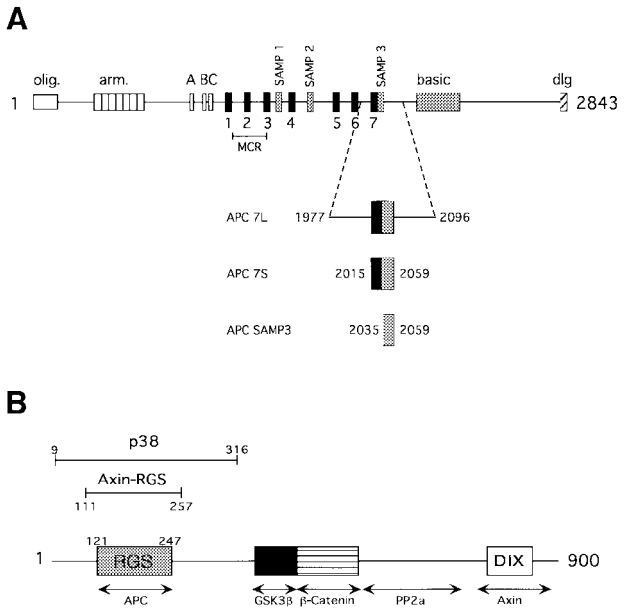

Fig. 1. Primary structure of the Axin and APC proteins. (**A**) Schematic of APC primary structure. The conserved oligomerization (olig.), armadillo repeat (arm.), basic and discs large interaction (dlg) domains are indicated. The 15 amino acid β-catenin-binding repeats are labeled A, B and C (white boxes). The 20 amino acid β-catenin-binding repeats are labeled 1–7 (black boxes). The Axin-binding repeats are labeled SAMP1–3 (gray boxes). Truncations in the midpoint cluster region (MCR) account for >60% of oncogenic mutations in APC (Miyoshi *et al*., 1992). The APC 7L, APC 7S and APC SAMP3 constructs used for binding assays are shown below the schematic and their boundaries are indicated. (**B**) Schematic of Axin primary structure showing regions identified by deletion experiments to be important for protein–protein interactions with APC, GSK3β, β-catenin and protein phosphatase 2a (PP2a). A region of homology to the DIX domain of Dishevelled has been implicated in Axin homodimerization. The region of sequence homology to RGS proteins is indicated. Bars indicate the regions corresponding to the thrombin-defined p38 fragment and the elastase-defined Axin-RGS fragment.

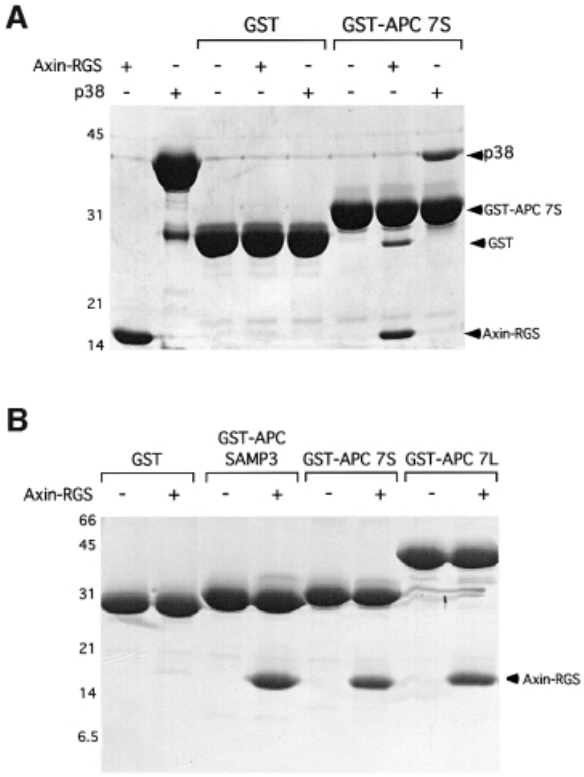

Fig. 2. Identification of minimal interaction domains of APC and Axin. (**A**) Binding of the Axin-RGS and p38 fragments to the GST–APC 7S fusion protein. Lane 1, 1 nmol Axin-RGS; lane 2, 1 nmol p38; lanes 3–8, GST pull-down assays containing Axin-RGS, p38, GST and GST–APC 7S as indicated. The GST in lane 7 is a result of cleavage of the fusion protein by a thrombin contaminant in the Axin-RGS preparation. (**B**) Binding of Axin-RGS to the GST–APC SAMP3, GST–APC 7S and GST–APC 7L constructs.

Axin functions as a scaffold on which multiple proteins assemble to regulate β-catenin stability.

Studies of fragments of APC and Axin have identified the regions of these proteins that are involved in their interaction. The region of Axin involved in APC binding has significant homology to members of the regulators of G-protein signaling (RGS) family (Zeng *et al*., 1997; Ikeda *et al*., 1998; Kishida *et al*., 1998), but does not regulate any of the known G-proteins (Mao *et al*., 1998). The region of APC implicated in binding the Axin homolog conductin consists of a conserved sequence of ~20 amino acids containing a Ser-Ala-Met-Pro motif (Behrens *et al*., 1998). APC contains three repeats of this sequence, designated 'SAMP repeats', which are distributed among the seven 20 amino acid β-catenin-binding repeats of APC (Figure 1A). Most oncogenic mutants of APC truncate the protein prior to the SAMP repeats, but preserve some of the β-catenin-binding repeats and β-catenin-binding activity (Miyoshi *et al*., 1992; Rubinfeld *et al*., 1997a) (Figure 1A), suggesting an important role for Axin binding in APC tumor suppressor function.

To understand further the interaction between Axin and APC, we have determined the crystal structure of the RGS domain of Axin (Axin-RGS) alone and in complex with the third SAMP repeat (SAMP3) of APC. The structures reveal that the SAMP3 peptide binds on the opposite face of the protein from the G-protein-binding site of traditional RGS domains. The contacts between the two proteins appear to be conserved in diverse species. Mutation of several conserved residues from Axin-RGS provides further insight into the molecular nature of the Axin–APC interaction.

Results and discussion

Analysis of APC binding by protease-resistant Axin fragments

Deletion mutagenesis studies have mapped the APC-binding site of Axin to the RGS homologous region (Behrens *et al*., 1998; Hart *et al*., 1998; Kishida *et al*., 1998). In order to assess whether this APC-binding activity corresponds to a discrete, physical domain of Axin, bacterially expressed Axin was subjected to partial proteolysis followed by N-terminal sequencing and mass spectrometry (data not shown). Two fragments of Axin that contain the RGS homology region were obtained (Figure 1B). The longer of the two fragments, which we call p38, is a thrombin digestion product that extends from residue 9 to residue 316, 70 residues beyond the RGS homology region. A shorter, elastase-resistant fragment (residues 111–257) essentially corresponds to the boundaries of the RGS domain identified by sequence homology

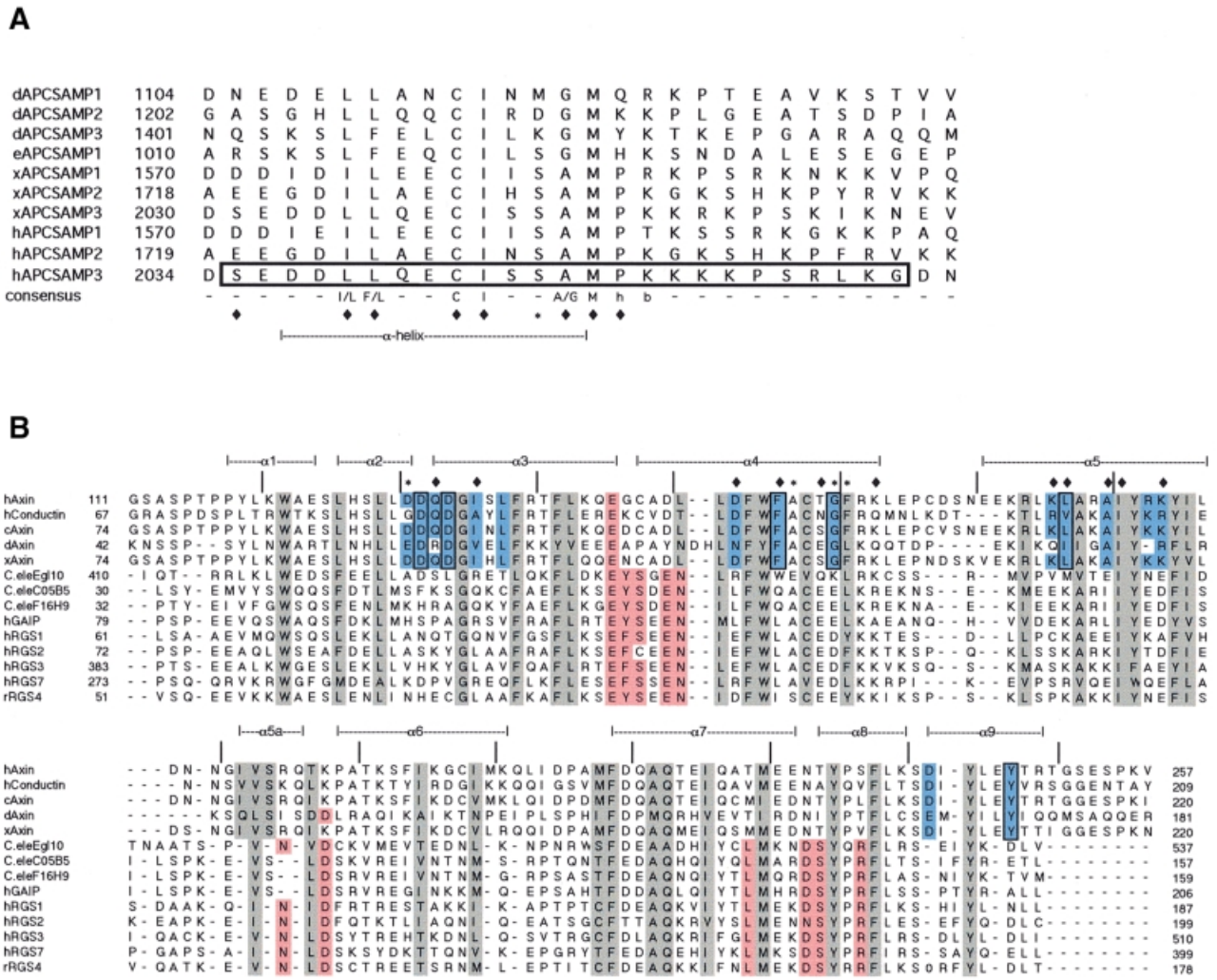

Fig. 3. Conservation of SAMP repeats and RGS domains. (**A**) Alignment of the SAMP repeats of *Drosophila* APC (dAPC), *Drosophila* APC2 (eAPC), *Xenopus* and human APC. Starting residue numbers for within the full-length proteins are indicated. The SAMP3 sequence used in crystallization is boxed. Residues that contact Axin-RGS in the RGS–SAMP3 complex structure are indicated by a diamond (contacts by side chain atoms) or an asterisk (contacts by main chain atoms only) below the alignment. A consensus sequence is given (h, hydrophobic; b, basic), and the residues that form the α-helical portion of the peptide are indicated. (**B**) Structure-based alignment of Axin-RGS and RGS4 with other RGS family members. Conserved hydrophobic core residues are highlighted in gray, residues determined to contact $G_{i\alpha}$ in the RGS4–$G_{i\alpha}$ complex structure (Tesmer *et al*., 1997) are in pink. Conserved Axin subfamily residues are light blue. Residues that contact SAMP3 in the RGS–SAMP3 complex structure are indicated by symbols above the alignment, as in (A). Those residues changed in human Axin in the mutagenesis experiments are boxed. Secondary structure elements observed in Axin-RGS are indicated above the alignment (α1–α9), and tick marks indicate every 10 residues in human Axin. Axin family members shown are: human Axin (crystal structure in this paper, DDBJ/EMBL/GenBank accession No. AAC51624), human conductin (NM004655), chicken Axin (AF009012), *Drosophila* Axin (AF086811) and *Xenopus* Axin (AF097313). Other RGS family members are *Caenorhabditis elegans* Egl10 (CEU32326), C05B5 (Z32679) and F16H9 (Z50005), human GAIP (NM005873), human RGS 1 (NM002922), 2 (NM002923), 3 (HSU27655) and 7 (U32439) and rat RGS4 (AF117211).

(residues 121–247) (Figure 1B). We will refer to this fragment as Axin-RGS. A fragment of APC containing β-catenin-binding repeat 7 and the third SAMP repeat bound equally well to the Axin-RGS and p38 proteins (Figure 2A). The 147 amino acid RGS domain of Axin therefore contains the minimal APC-binding site, as expected from earlier work (Behrens *et al*., 1998; Hart *et al*., 1998; Kishida *et al*., 1998).

Previous studies have shown that the SAMP repeats are necessary for APC binding to Axin/conductin. All fragments of APC that bind Axin or conductin contain at least one SAMP repeat (Behrens *et al*., 1998; Hart *et al*., 1998), and mutation of the Ser-Ala-Leu-Pro sequence in one such fragment to Ala-Ala-Leu-Pro abolishes conductin binding (Behrens *et al*., 1998). However, each of the fragments used in these experiments is substantially larger than the SAMP repeat alone. Thus, it is unclear whether a single SAMP repeat is sufficient for Axin binding in the absence of any flanking sequence. In order to identify a minimal fragment of APC with full Axin-binding activity *in vitro*, we constructed a series of truncations in APC (Figure 1A). Beginning with a construct spanning those used previously (APC 7L, see Figure 1A), we compared the Axin-RGS-binding activity of each truncation in glutathione *S*-transferase (GST) pull-down assays. A GST fusion of the 25 amino acid APC SAMP3 repeat alone bound to Axin-RGS as well as the longest fragment tested (Figure 2B). No binding to the GST control was seen.

Table I. Crystallographic statistics

	Axin-RGS	RGS–SAMP3
Data collection[a]		
resolution (Å)	29.3–1.57	32.0–1.90
space group	$C222_1$	$P2_12_12_1$
unit cell dimensions (Å)		
a	32.57	30.60
b	117.88	69.98
c	81.90	71.96
R_{merge}[b]	5.1 (18.6)	5.0 (29.5)
% >3σ(*I*)	81.0 (56.8)	81.2 (51.4)
completeness (%)	99.1 (99.1)	99.3 (99.7)
average redundancy	3.6 (3.0)	3.2 (3.0)
Refinement		
R values and temperature factors		
number of reflections		
working set	20127	10870
test set	2211	1199
R_{cryst}[d]	0.172	0.206
R_{free}[d]	0.197	0.222
average *B* (Å^2)		
protein	15.3	27.4
solvent	37.0	55.5
main chain bond-related *B* r.m.s.d	1.5	2.0
main chain angle-related *B* r.m.s.d	2.2	2.9
side chain bond-related *B* r.m.s.d	2.1	2.7
side chain angle-related *B* r.m.s.d	3.2	4.4
Model geometry		
bond length r.m.s.d. from ideal (Å)	0.007	0.006
bond angle r.m.s.d. from ideal (°)	1.45	1.12
Ramachandran plot		
% in most favored regions	93.9	91.9
% in additional allowed regions	6.1	8.1

[a]Values in parentheses are for the highest resolution shell (1.59–1.57 Å for Axin-RGS, 1.93–1.90 Å for RGS–SAMP3).
[b]$R_{merge} = 100 \times \Sigma|I - \langle I\rangle|/\Sigma\langle I\rangle$.
[c]The test set comprises a randomly selected subset of the data (9.9% of each set) that was not included in the refinement of the model. The working set contains the remaining reflections from the data set.
[d]$R = \Sigma_h||F_{obs}(h)| - |F_{calc}(h)||/\Sigma_h|F_{obs}(h)|$. R_{cryst} and R_{free} were calculated using the working and test reflection sets, respectively.

Hence, this 25 amino acid fragment of APC is sufficient for full Axin binding. This fragment encompasses the conservation seen among SAMP repeats (Figure 3A).

Axin-RGS domain structure

Axin-RGS was crystallized and its structure determined by molecular replacement, using the structure of RGS4 (Tesmer *et al*., 1997) as a search model. RGS4 is 28% identical in amino acid sequence to Axin-RGS (Figure 3B), and its structure has been solved in complex with the G-protein $G_{i\alpha}$ (Tesmer *et al*., 1997). The Axin-RGS structure was refined to a maximum resolution of 1.57 Å (Table I). In general, the electron density is extremely well defined (Figure 4A) and the final model contains all residues present in the protein. However, no electron density was seen for Ser114, despite very clear electron density on both sides of this residue. This may be a result of alternative backbone positions at position 114, but attempts to model alternative conformations failed.

Not surprisingly, the structure of Axin-RGS strongly resembles that of RGS4 (Figure 4B). The root-mean-square deviation (r.m.s.d.) of the 111 common C_α positions after superimposing the domains is 1.3 Å, and Axin-RGS contains the nine α-helices observed in RGS4.

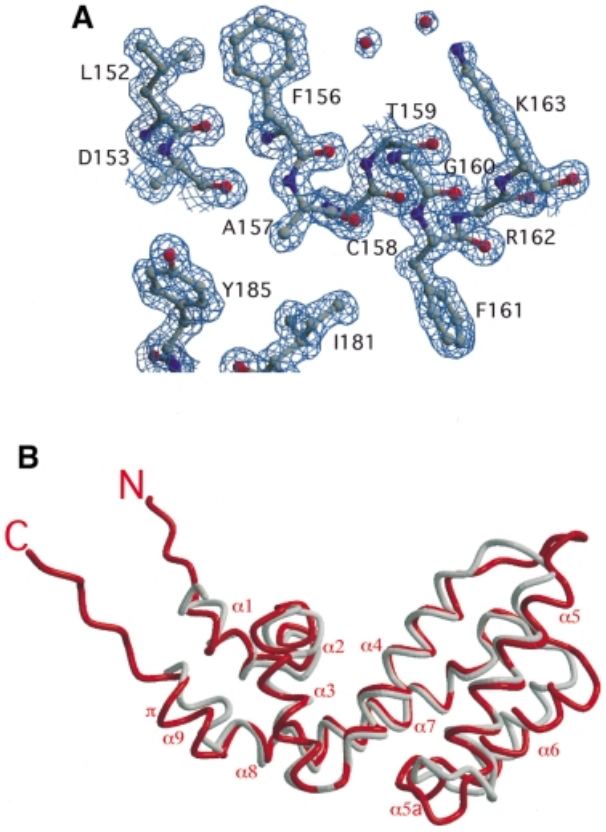

Fig. 4. Structure of Axin-RGS. (**A**) Final Axin-RGS $2F_o - F_c$ α-calc electron density map in the region of surface-exposed, conserved residues Phe156 and Gly160. The map is contoured at 1.2σ. (**B**) Comparison of Axin-RGS with RGS4. Axin-RGS is red, RGS4 is gray. Helices are labeled as in Figure 3B. The additional helix of Axin-RGS (α5a) and the turn of the π-helix (π) are indicated.

However, the loop positions within the two structures are quite different and Axin-RGS contains one additional, short α-helix in what is a $G_{i\alpha}$-interacting loop of RGS4 (helix 5a, see Figure 4B). In addition, helix 9 of Axin-RGS contains one turn of rarely observed π-helix (residues 242–249), whereas the corresponding helix in RGS4 appears to be purely α-helical. The recently published solution structure of another RGS protein, Gα-interacting protein (GAIP), reveals a similar overall fold to RGS4 and Axin-RGS (de Alba *et al*., 1999).

RGS–SAMP3 complex structure

The structure of Axin-RGS in complex with the 25 amino acid SAMP3 repeat (Figures 1A and 3A) of APC (RGS–SAMP3) was determined by molecular replacement using Axin-RGS as a search model (Table I; see Materials and methods). The structure was refined to a resolution of 1.9 Å (Figure 5A). Residues 117–248 of Axin-RGS and 2035–2050 of APC are visible, whereas the N- and C-termini of Axin-RGS and the C-terminus of SAMP3 appear to be disordered. There is no conformational change between the bound and unbound forms of Axin-RGS: the C_α r.m.s.d. of the superimposed domains, ignoring flexible loops involved in crystal contacts (see Materials and methods), is 0.56 Å.

The SAMP3 peptide binds a face of Axin-RGS opposite the $G_{i\alpha}$-binding site of RGS4 (Figure 5B). Comparison of

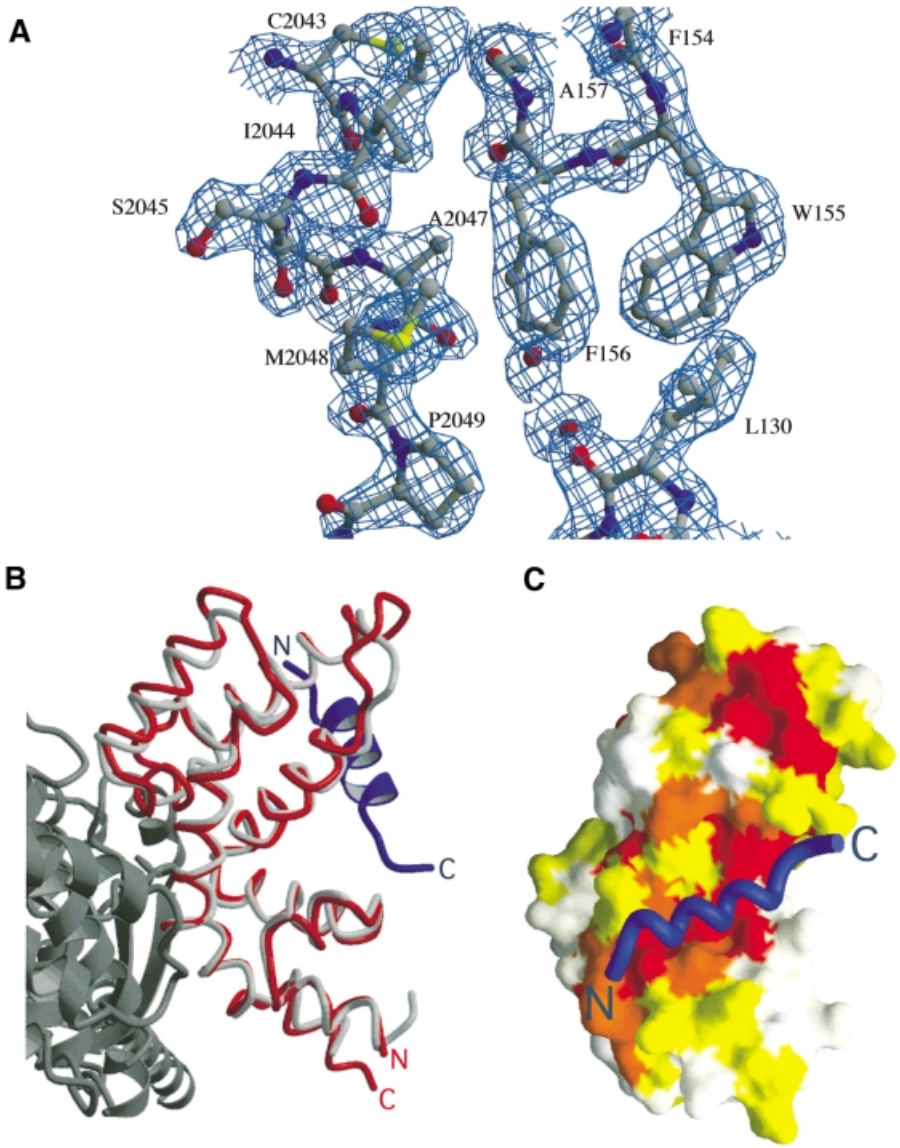

Fig. 5. Structure of the RGS–SAMP3 complex. (**A**) Final RGS–SAMP3 $2F_o - F_c$ α-calc electron density map in the region of SAMP3 residues Cys2043–Pro2049. The map is contoured at 1σ. (**B**) The SAMP3-binding site of Axin-RGS is distinct from the $G_{i\alpha}$-binding site of RGS4. The Axin-RGS–SAMP3 complex is superimposed on the structure of the RGS4–$G_{i\alpha}$ complex. Axin-RGS is red, SAMP3 is blue, RGS4 is light gray and $G_{i\alpha}$ is dark gray. The complex is rotated 90° perpendicular to the page, then 180° around the vertical relative to the orientation of Axin-RGS in Figure 4B. (**C**) Conservation of the APC-binding surface of Axin-RGS. Surface representation of Axin-RGS, colored by conservation of residues within Axin family members. White indicates that a residue is not significantly conserved, yellow and orange indicate residues that are conserved or conservatively substituted, and red indicates residues that are absolutely conserved in Axin homologs. The SAMP3 peptide C_α trace is drawn in blue. The second conserved patch referred to in the text is visible near the top of Axin-RGS, above the SAMP3-binding site. The complex is rotated 180° around the horizontal relative to its orientation in (B).

Axin subfamily RGS domain sequences from diverse species reveals that those residues that form the SAMP3-binding site of Axin-RGS are highly conserved in these APC-binding RGS domains (Figures 3B and 5C), but are not conserved in other RGS proteins (Figure 3B). Several of these residues were previously identified by phylogenetic analysis as being characteristic of the Axin subfamily of RGS proteins (Zheng *et al.*, 1999). Similarly, many of those residues that contact $G_{i\alpha}$ in the RGS4–$G_{i\alpha}$ structure do not appear to be conserved in Axin subfamily RGS domains (Figure 3B). Thus, it appears that the Axin subfamily uses the RGS fold as a structure on which to build a unique binding surface, rather than adapting the interactions used in classical RGS–G-protein binding.

Residues from SAMP3 that contact Axin-RGS appear to be conserved both within and between species (Figures 3A and 6A–C). From Asp2037 to Ala2047, the SAMP3 peptide binds to Axin-RGS as an α-helix, with a repeating pattern of two residues contacting Axin-RGS, and two facing out into solution. The evolutionary conservation of SAMP repeats follows this pattern, with those residues that face in and contact Axin-RGS highly conserved, and those that face out much more variable (Figure 3A). Leu2039

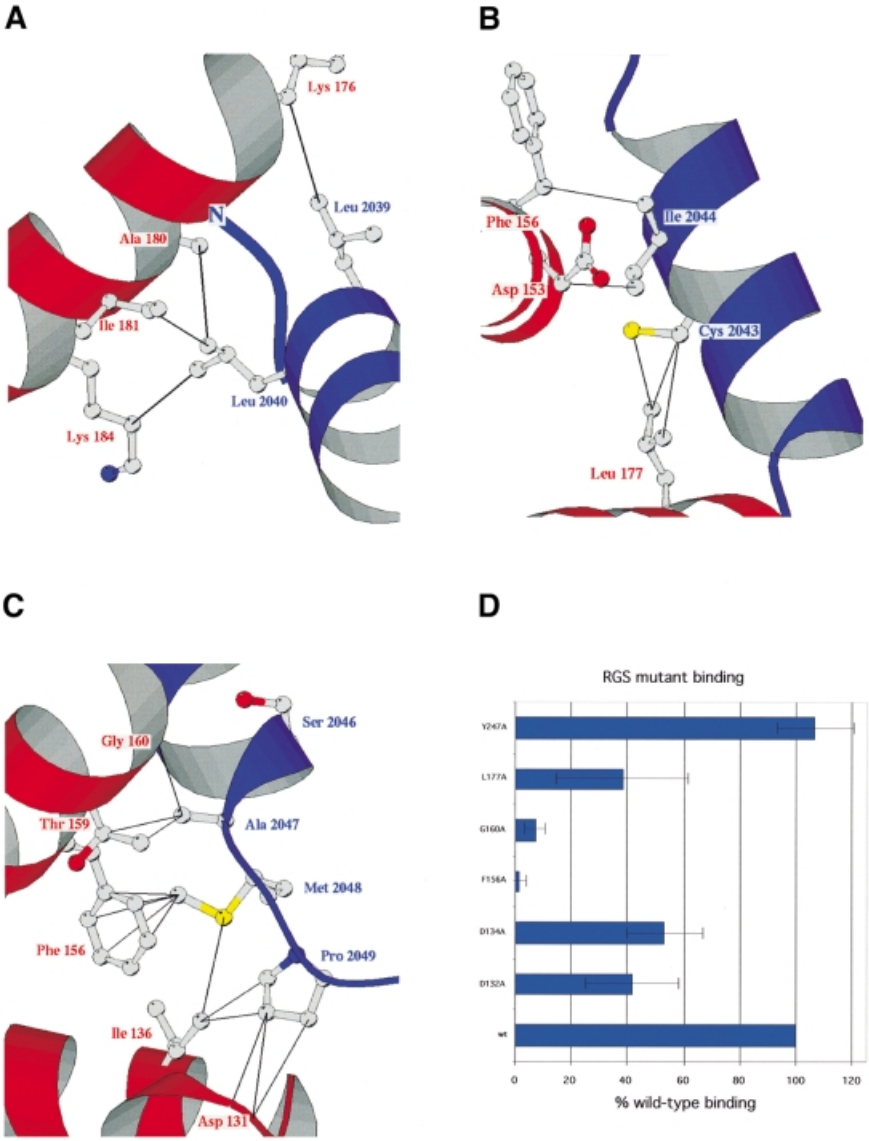

Fig. 6. The molecular interactions between Axin-RGS and SAMP3. (**A**) Interactions of SAMP3 Leu2039 and Leu2040 with Axin-RGS. Protein backbones are colored red for Axin-RGS or blue for SAMP3, and residue numbers are labeled using the same color scheme. Side chains are colored by atom type (carbon, gray; nitrogen, blue; oxygen, red; sulfur, yellow). Solid black lines indicate hydrophobic contacts. The orientation of the complex is as in Figure 5B. (**B**) Interactions of SAMP3 Cys2043 and Ile2044 with Axin-RGS. Coloring is as in (A). The complex is rotated 180° around the horizontal relative to its orientation in Figure 5B. (**C**) Interactions of the characteristic Ser-Ala-Met-Pro sequence of SAMP3 with Axin-RGS. Coloring is as in (A) and (B). Orientation is as in Figure 5B. (**D**) Effects of mutation of conserved Axin-RGS residues on SAMP3 binding. Graph shows mean ± SD of four binding assays for each mutant, plotted as a percentage of wild-type binding.

and Leu2040, which form hydrophobic contacts with Axin-RGS (Figure 6A), are conserved as hydrophobic residues in both vertebrate and *Drosophila* SAMP repeats (Figure 3A). Cys2043 and Ile2044, which are involved in many more residue-specific contacts (Figure 6B), are conserved as a cysteine and an isoleucine in all known SAMP repeats (Figure 3A).

Perhaps most interesting are the binding interactions in the region of the Ser-Ala-Met-Pro sequence that originally defined the SAMP repeats (Figure 6C). Although this sequence is absolutely conserved in all vertebrates, it is highly diverged in the *Drosophila* sequences (Figure 3A). Ser2046, which does not form any side chain-mediated Axin-RGS contacts, is not conserved. Ala2047 forms a number of close contacts with residues from Axin-RGS, suggesting that a small residue is essential at this position. This residue is consistently replaced by glycine in the *Drosophila* SAMP repeats (Figure 3A), which may be a result of the replacement of Thr159 of Axin-RGS with a larger glutamate in *Drosophila* Axin (Figure 3B). Surprisingly, Pro2049, which forms several hydrophobic contacts with Axin-RGS through its side chain methylene groups, is not conserved in the *Drosophila* SAMP repeats (Figure 3A). However, it is replaced in all cases by a residue containing carbons at the equivalent positions. This may be a consequence of repacking in this area, due to the replacement of Axin-RGS Asp131 and Ile136 with glutamate and valine, respectively, in the *Drosophila* Axin sequence (Figure 3B). Of the sequence for which the SAMP repeats are named, only the methionine residue

(Met2048 of SAMP3), which forms numerous hydrophobic contacts through its sulfur atom and terminal methyl group (Figure 6C), is conserved in *Drosophila* SAMP repeats. In the study that originally identified the SAMP repeats (Behrens *et al*., 1998), mutation of the Ser-Ala-Met-Pro sequence to Ala-Ala-Leu-Pro abolished binding of APC to the Axin homolog conductin. The crystal structure suggests that the Met→Leu mutation is responsible for the observed loss of binding in this double mutant, as the shorter leucine residue would be unable to form those contacts made by the terminal methyl group of methionine. The lack of contacts between Ser2046 and Axin-RGS suggests that mutation of serine to alanine would have little effect on binding.

The RGS–SAMP3 structure also provides insights into the conservation of Axin-binding repeats in diverse species. Previous work has identified sequences from *Drosophila* APC (dAPC) and APC2 (eAPC) that have homology to the SAMP repeats of vertebrate APC (Hamada *et al*., 1999; McCartney *et al*., 1999; Yu *et al*., 1999). However, the distant homology between these sequences and those of vertebrate SAMP repeats have made it difficult to identify these sequences unambiguously as Axin-binding sites in the absence of functional studies. The conservation of those residues observed to make contacts in the RGS–SAMP3 complex supports the theory that three such sequences from dAPC and one from eAPC are Axin-binding sites (Figure 3A).

To assess the role of individual residues in the binding interaction, we studied the binding activity of point mutants in conserved Axin-RGS residues (Figure 6D). Replacement of Phe156 with Ala reduced binding to nearly undetectable levels, whereas Leu177→Ala mutation reduced binding to about one-third of normal. Both of these residues make hydrophobic contacts with SAMP3 (Figure 6B and C). Phe156→Ala mutation would be expected to disrupt six hydrophobic contacts, while Leu177→Ala mutation would disrupt only three. Hence, it is not surprising that the former mutation had a greater effect on binding than the latter. Addition of a single methyl group to Gly160 nearly abolished binding. Gly160 sits in a very tightly packed region of the complex, and forms close contacts with several residues from the SAMP3 peptide, including the conserved Ala2047 residue (Figure 6C). The presence of the additional methyl group in the Gly160→Ala mutant would be expected to create a steric clash that would greatly reduce binding.

In addition to the SAMP3-binding region, a second conserved patch is present on the Axin-RGS surface (Figures 3B and 5C). This patch consists of Asp132, Asp134, Asp242, Leu138 and Tyr247. We investigated the roles of several of these residues in binding using mutagenesis. Tyr247→Ala mutation had no effect on binding (Figure 6D), as expected. However, mutation of Asp132 or Asp134 to alanine reduced binding by ~50%. It is possible that the conserved Asp132 and Asp134 residues interact with the basic residues in the C-terminus of the SAMP3 peptide, which are disordered in the complex structure (Figure 3A). As the cocrystals were grown at pH 5.5, we hypothesized that such an interaction may be disrupted by protonation of the acidic side chains under the conditions used for crystallization. However, adaptation of the crystals to neutral pH did not affect the complex structure (see Materials and methods). It is possible that the constraints of the crystal environment could prevent rearrangement of the peptide conformation in the pH-adapted crystals. However, this is unlikely, as the crystal is not very tightly packed in this region. It seems more likely that Asp132 and Asp134 participate in a general electrostatic, rather than a direct, interaction with the C-terminal basic residues of SAMP3, or that the aspartates help to position nearby residues 130, 131 and 133, which form contacts with Pro2049 of SAMP3 (Figure 6C). A more interesting possibility is that this conserved patch plays a role in the ternary Axin–APC–β-catenin complex. Such a role would most likely be through an Axin–APC interaction that is stabilized in the presence of β-catenin, as direct Axin-RGS–β-catenin interaction has never been observed.

The regulation of β-catenin stability by Axin and APC is critical for both development and cancer prevention. The studies presented here provide a framework for understanding the molecular nature of this essential process. However, a structure of the Axin–APC–β-catenin ternary complex will ultimately be required for a more detailed understanding of the molecular interactions that mediate complex formation and β-catenin degradation.

Materials and methods

Expression and purification of proteins

To produce p38, amino acids 9–600 of human Axin were overexpressed in *Escherichia coli* BL 21 cells as a thrombin-cleavable C-terminal fusion to GST using the pGEX-KG vector (Guan and Dixon, 1991). Cells were grown at 37°C to an OD of 0.5–0.8, induced with isopropyl-β-D-thiogalactopyranoside (IPTG) to a concentration of 0.2 mM, and further grown at 37°C for another 3–5 h. Cells were lysed by pressing once using a SLM-AMINCO French Press at a maximum pressure of 1200 psi, and lysates were spun at 300 000 *g* for 30 min at 4°C to remove any insoluble material. Protein was batch purified on glutathione–agarose beads (10 ml beads per liter of original culture). Thrombin cleavage of the GST tag was performed using 1.5 U of thrombin (Sigma) per ml of beads, at 22°C for 1 h. This resulted in an internal cleavage of human Axin, liberating a fragment that migrated at ~38 kDa on SDS–PAGE. N-terminal sequencing and mass spectroscopy identified this fragment as containing residues 9–316 of human Axin. The fragment was purified by anion exchange chromatography (Mono Q; Pharmacia) in a buffer containing 25 mM Tris pH 8.5, 2 mM dithiothreitol (DTT) with elution by an NaCl gradient. Size exclusion chromatography (Superdex 200 HR; Pharmacia) in 25 mM Tris pH 8.5, 150 mM NaCl, 2 mM DTT was used for further purification. Both chromatography steps were performed at 4°C. Pure fractions were concentrated using an Amicon Centriprep-10 concentrator (10 000 Da mol. wt cut-off).

Expression and purification of the wild-type and mutant Axin-RGS proteins were as for p38, except that the pGEX-2T vector (Pharmacia) was used and cleavage was with 4 U of thrombin per ml of beads for ≥2 h. Axin-RGS does not bind to the Mono Q column at pH 8.5; however, thrombin does bind to the column, so the Axin-RGS-enriched Mono Q flow-through was collected, concentrated as above and loaded on to the gel filtration column. Gel filtration fractions containing pure Axin-RGS were concentrated as above and used directly for crystallization trials, or frozen with liquid nitrogen in small aliquots for use in binding assays. Freezing did not affect the binding by APC (data not shown).

APC constructs were also expressed as GST fusion proteins in pGEX-KG and purified by batch affinity on glutathione–agarose beads as above. Fusion proteins were eluted at 22°C using a buffer containing 25 mM MES pH 5.5, 150 mM NaCl, 2 mM DTT and 50 mM reduced glutathione. Fractions containing protein were identified using a Bradford assay, exchanged into a low-salt buffer, and purified by cation exchange (Mono S; Pharmacia) in MES buffer pH 5.5, 2 mM DTT with an NaCl gradient. All steps of APC purification were performed in the presence of 0.4 mM phenylmethylsulfonyl fluoride (PMSF), 2 mM EDTA, 2 μg/ml aprotinin, 2 μg/ml pepstatin A, 1 μg/ml leupeptin and 0.5 μg/ml E64. Ion

exchange and size exclusion chromatography were carried out at 4°C. Protein was concentrated and frozen in small aliquots as described above. Again, it was shown that freezing had no effect on binding (data not shown).

The SAMP3 peptide used in crystallization was produced by Fmoc synthesis and lyophilized. The lyophilized peptide was resuspended to 10 mg/ml in 20 mM sodium phosphate pH 4.4, 5% acetonitrile and purified on a Vydac C_{18} HPLC column, using a 5–70% acetonitrile gradient in 20 mM sodium phosphate pH 4.4. Pure fractions were pooled, evaporated in a Speedvac and lyophilized. Pure peptide was then resuspended in water, desalted using a G15 Sephadex (Sigma) column and relyophilized.

Elastase digestion

Twenty milligrams of Axin p38 were incubated with 6.2, 25, 50, 100, 200, 400, 800 or 1600 ng of elastase at room temperature, in a total volume of 15 µl containing 50 mM Tris pH 8, 2 mM $CaCl_2$ and 1 mM DTT. After 10 min, reactions were stopped by adding 2 µl of 0.1 M PMSF. Loading dye was added to samples, which were boiled and loaded on to an SDS–polyacrylamide gel. Fragments corresponding to Axin-RGS accumulated in 100–1600 ng elastase digests.

Crystallization

Axin-RGS crystals resembling clusters of needles and stacks of thin plates were obtained using the hanging drop vapor diffusion method and 5 mg/ml Axin-RGS stock in 1.6 M $(NH_4)_2SO_4$, 75 mM NaOAc pH 4.25, 5% glycerol, 4 mM DTT at 4°C. Microseeds were prepared using serial dilutions of washed, crushed crystals into 1.6 M $(NH_4)_2SO_4$, 75 mM NaOAc pH 4.25, 4 mM DTT. Drops were prepared by mixing 1 µl of seed stock with 1 µl of protein stock and 2 µl of well solution. Seeding using a 10^{-3} dilution of seeds, 16 mg/ml Axin-RGS and a well solution of 1.2 M $(NH_4)_2SO_4$, 50 mM NaOAc pH 4.25, 30% glycerol, 4 mM DTT at 4°C yielded single plates and stacks of plates. The dimensions of the crystal used for data collection were 200 × 200 × 5 µm.

Crystals of RGS–SAMP3 were obtained from a solution 1 mM in each of Axin-RGS and SAMP3 peptide. The two proteins were incubated at 4°C for ⩾1 h before use in crystallization trials. Crystals resembling single rods and clumps of rods grew to maximum dimensions of 20 × 20 × 500 µm using the hanging drop vapor diffusion method, with a well solution containing 50 mM MES pH 5.5, 42.5% polyethylene glycol (PEG) 400, 15% glycerol and 5 mM DTT. Data were collected for two crystals, one at pH 5.5 and one adapted to pH 7.0 by transferring it to 50 mM MES pH 6.0, 45% PEG 400, 20% glycerol, 5 mM DTT for 30 min, then to the same solution at pH 6.5 for 30 min, then to pH 7.0 (HEPES buffer) for 3 days. The approximate dimensions of the pH 5.5 crystal were 10 × 10 × 200 µm, while those of the pH-adapted crystal were 10 × 10 × 400 µm.

Data collection and processing

Axin-RGS data (Table I) were collected from a single crystal at beamline 9-1 of the Stanford Synchrotron Research Laboratory (SSRL) (wavelength 0.98 Å). The crystal was frozen directly in a 100 K liquid nitrogen stream without additional cryoprotection. A total of 80° of data were measured, using a two-pass strategy on an MAR 345 imaging plate in 180 mm mode. High-resolution data (1.57 Å) were measured at a crystal–detector distance of 120 mm, with a 40 s exposure per 1° oscillation. Low-resolution data (29.3–2.9 Å) were measured at a distance of 250 mm, with a 15 s exposure per 2.5° oscillation. There is one Axin-RGS molecule per asymmetric unit, with a solvent content of 48%.

RGS–SAMP3 pH 5.5 data (resolution 2.2 Å, R_{merge} 0.033, completeness 89.1%) were collected at SSRL beamline 9-2 (wavelength 0.98 Å). The crystal was frozen directly as above. A total of 82.5° of data were measured, using a 100 s exposure per 1° oscillation on an ADSC Quantum4 CCD detector. The crystal–detector distance was 175 mm. Unit cell dimensions were 30.46 × 69.60 × 72.21 Å. RGS–SAMP3 pH 7.0 data (Table I) were collected at SSRL beamline 9-1 (wavelength 0.97 Å). The crystal was frozen directly as above. A total of 85° of data were measured, using a 90 s exposure per 1° oscillation on a MAR 345 imaging plate in 180 mm mode. The crystal–detector distance was 160 mm. There is one Axin-RGS molecule per asymmetric unit, with a solvent content of 39%.

All diffraction data were processed and scaled using DENZO and SCALEPACK (Otwinowski and Minor, 1997).

Phasing, model building and refinement

Phases for the Axin-RGS structure were determined by molecular replacement, using the CCP4 (Collaborative Computational Project, 1994) version of the program AMoRe (Navaza, 1994). The search model consisted of the RGS4 structure (Tesmer *et al*., 1997), with non-identical residues replaced by alanine (90 alanines of 128 total residues). The top solution from the rotation search (resolution 15–3.5 Å) was 4.4σ and the second highest solution was 3.9σ above the mean. The top four translation function solutions all resulted from the top rotation function solution. The best solution had a correlation coefficient of 0.526 and an *R*-factor of 0.502 after rigid-body refinement, whereas the next three solutions had correlation coefficients/*R*-factors of 0.467/0.534, 0.466/0.532 and 0.447/0.533. A 2.8 Å resolution electron-density map was calculated using phases from the top translation function solution, and used for model building in O (Jones *et al*., 1991). A random 10% of the data were removed before refinement and constituted the test set for cross-validation (Brünger, 1992). The model was refined in CNS (Brünger *et al*., 1998) using a maximum-likelihood amplitude target (Pannu and Read, 1996). Overall anisotropic temperature factor and bulk solvent corrections were applied throughout the refinement (Sheriff and Hendrickson, 1987). Refinement consisted of two rounds of simulated annealing, interspersed with rounds of minimization, followed by further minimization and temperature factor refinement. In the late rounds of refinement, occupancies of some water, sulfate and glycerol molecules were refined. Model geometry was monitored using PROCHECK (Laskowski *et al*., 1993). The final model includes 147 amino acids (13 in alternative side chain conformations), 178 water molecules (three in alternative locations), six sulfate ions (one in alternative locations), five glycerol molecules and one DTT molecule.

For the RGS–SAMP3 pH 5.5 complex, phases were determined by molecular replacement in CNS (Brünger *et al*., 1998), using the Axin-RGS structure as a search model. The top solution from the rotation function was 6.1σ above the mean, while the second solution was 2.9σ above the mean. The top solution from the translation function had a correlation coefficient of 0.434. The next best non-equivalent solution had a correlation coefficient of 0.209. The structure was refined in CNS to an R/R_{free} of 0.197/0.243. Phases for the pH 7.0 complex were generated using rigid-body minimization with the pH 5.5 structure (initial R/R_{free} = 0.289/0.303), and the structure was refined in CNS as above, but without simulated annealing and occupancy refinement steps. The final model includes 132 amino acids (four in alternative side chain conformations, four in alternative backbone conformations), 61 water molecules and seven glycerol molecules.

Structure comparison

C_α r.m.s.d. for the various structures was calculated using O (Jones *et al*., 1991). There were no major differences between the pH 5.5 and pH 7.0 structures: the C_α r.m.s.d for all residues visible in both structures (residues 117–248) is 0.19 Å. The C_α r.m.s.d. for all residues visible in both the Axin-RGS and RGS–SAMP3 structures is 0.85 Å. Exclusion of those residues whose positions are likely to be influenced by crystal contacts resulted in a C_α r.m.s.d. of 0.56 Å for 89 residues (125–142, 151–163, 172–186, 193–208 and 220–246), including all residues involved in contacts with SAMP3.

GST pull-down experiments

GST fusion protein (5 nmol) was combined with 15 nmol of Axin-RGS or p38 and 50 µl (bed volume) of glutathione–agarose beads in a total volume (including beads) of 250 µl. Protein concentrations were determined by absorbance at 280 nm, using extinction coefficients calculated from the protein sequence (Creighton, 1995). Proteins and beads were incubated for ⩾1 h at 4°C in the presence of 50 mM HEPES pH 7.0, 150 mM NaCl, 0.05% Tween-20, 2 mM DTT and 1 mM PMSF. Beads were washed four times with 1 ml of the same buffer, resuspended in SDS loading buffer, and loaded to SDS–polyacrylamide gels for analysis.

Quantification in GST pull-down assays

Integrated intensities of bands on SDS–polyacrylamide gels were obtained using the NIH Image program (developed at the US National Institutes of Health and available on the Internet at http://rsb.info.nih.gov/nih-image/). Variations in gel loading were corrected by converting intensities to an Axin-RGS:GST–APC ratio within each lane. For each binding assay, the Axin-RGS:GST–APC ratio of each mutant was divided by the ratio in the wild-type lane, to correct for any differences in wash stringency or intensity of Coomassie staining. Results were plotted as the mean percentage wild-type binding, plus or minus one standard deviation. Figure 6D shows the mean and standard deviation of four trials, three using the GST–APC 7S construct and one using the GST–APC 7M

construct (APC residues 1994–2080). These trials encompass two separate preparations of each mutant protein.

Axin-RGS mutagenesis

Mutagenesis was performed using the QuikChange kit (Stratagene), according to the manufacturer's instructions. All mutant constructs were verified by DNA sequencing.

Illustrations

Figures 4A and B, and 5A and B were generated using BOBSCRIPT (Kraulis, 1991; Esnouf, 1997) and RASTER3D (Merritt and Murphy, 1994). Figure 6A–C was generated using BOBSCRIPT. Figure 5C was created using GRASP (Nicholls *et al*., 1993). The alignment in Figure 3B was performed originally in CLUSTALW, and adjusted by hand using the structures of Axin-RGS and RGS4 (Tesmer *et al*., 1997). Accessible surface area calculations were performed in CNS (Brünger *et al*., 1998). Hydrophobic core residues were defined as 95% burial of a residue or significant burial of side chain carbon atoms.

Coordinates and structure factors have been deposited with the Protein Data Bank under accession codes 1dk8 (Axin-RGS) and 1emu (RGS–SAMP3).

Acknowledgements

We thank K.Misura and A.May for assistance with data collection; B.Rubinfeld for technical assistance; H.Feinberg, A.Huber, A.May and S.Pokutta for helpful discussions; and S.Pokutta and A.May for comments on the manuscript. This work is based upon research conducted at the Stanford Synchrotron Radiation Laboratory (SSRL), which is funded by the Department of Energy (BES, BER) and the National Institutes of Health (NCRR, NIGMS). K.E.S. is a Howard Hughes Medical Institute Predoctoral Fellow. This work was supported by grant R01GM56169 to W.I.W. from the National Institutes of Health, the Pew Scholars Program in the biomedical sciences and a Stanford University/HHMI junior faculty award.

References

Behrens,J., Jerchow,B.A., Würtele,M., Grimm,J., Asbrand,C., Wirtz,R., Kühl,M., Wedlich,D. and Birchmeier,W. (1998) Functional interaction of an Axin homolog, conductin, with β-catenin, APC, and GSK3β. *Science*, **280**, 596–599.

Brannon,M., Gomperts,M., Sumoy,L., Moon,R.T. and Kimelman,D. (1997) A β-catenin/XTcf-3 complex binds to the *siamois* promoter to regulate dorsal axis specification in *Xenopus*. *Genes Dev.*, **11**, 2359–2370.

Brünger,A.T. (1992) Free *R* value: a novel statistical quantity for assessing the accuracy of crystal structures. *Nature*, **355**, 472–475.

Brünger,A.T. *et al*. (1998) Crystallography and NMR system: a new software suite for macromolecular structure determination. *Acta Crystallogr. D*, **54**, 905–921.

Collaborative Computational Project Number 4 (1994) The CCP4 suite: programs for protein crystallography. *Acta Crystallogr. D.*, **50**, 760–763.

Creighton,T.E. (1995) *Protein Structure: A Practical Approach*. IRL Press, New York, NY.

Dale,T.C. (1998) Signal transduction by the Wnt family of ligands. *Biochem. J.*, **329**, 209–223.

de Alba,E., De Vries,L., Farquhar,M.G. and Tjandra,N. (1999) Solution structure of human GAIP (Gα interacting protein): a regulator of G protein signaling. *J. Mol. Biol.*, **291**, 927–939.

Esnouf,R.M. (1997) An extensively modified version of Molscript that includes greatly enhanced coloring capabilities. *J. Mol. Graph.*, **15**, 132–137.

Fagotto,F., Jho,E., Zeng,L., Kurth,T., Joos,T., Kaufmann,C. and Costantini,F. (1999) Domains of Axin involved in protein–protein interactions, Wnt pathway inhibition, and intracellular localization. *J. Cell Biol.*, **145**, 741–756.

Fan,M.J., Grüning,W., Walz,G. and Sokol,S.Y. (1998) Wnt signaling and transcriptional control of *Siamois* in *Xenopus* embryos. *Proc. Natl Acad. Sci. USA*, **95**, 5626–5631.

Fukuchi,T., Sakamoto,M., Tsuda,H., Maruyama,K., Nozawa,S. and Hirohashi,S. (1998) β-catenin mutation in carcinoma of the uterine endometrium. *Cancer Res.*, **58**, 3526–3528.

Ginsburg,G.T. and Kimmel,A.R. (1997) Autonomous and nonautonomous regulation of axis formation by antagonistic signaling via 7-span cAMP receptors and GSK3 in *Dictyostelium*. *Genes Dev.*, **11**, 2112–2123.

Guan,K.L. and Dixon,J.E. (1991) Eukaryotic proteins expressed in *Escherichia coli*: an improved thrombin cleavage and purification procedure of fusion proteins with glutathione *S*-transferase. *Anal. Biochem.*, **192**, 262–267.

Hamada,F. *et al*. (1999) Identification and characterization of E-APC, a novel *Drosophila* homologue of the tumour suppressor APC. *Genes Cells*, **4**, 465–474.

Hart,M.J., de los Santos,R., Albert,I.N., Rubinfeld,B. and Polakis,P. (1998) Downregulation of β-catenin by human Axin and its association with the APC tumor suppressor, β-catenin and GSK3β. *Curr. Biol.*, **8**, 573–581.

He,T.C., Sparks,A.B., Rago,C., Hermeking,H., Zawel,L., da Costa,L.T., Morin,P.J., Vogelstein,B. and Kinzler,K.W. (1998) Identification of c-MYC as a target of the APC pathway. *Science*, **281**, 1509–1512.

Hsu,W., Zeng,L. and Costantini,F. (1999) Identification of a domain of Axin that binds to the serine/threonine protein phosphatase 2A and a self-binding domain. *J. Biol. Chem.*, **274**, 3439–3445.

Ikeda,S., Kishida,S., Yamamoto,H., Murai,H., Koyama,S. and Kikuchi,A. (1998) Axin, a negative regulator of the Wnt signaling pathway, forms a complex with GSK-3β and β-catenin and promotes GSK-3β-dependent phosphorylation of β-catenin. *EMBO J.*, **17**, 1371–1384.

Ilyas,M., Tomlinson,I.P., Rowan,A., Pignatelli,M. and Bodmer,W.F. (1997) β-catenin mutations in cell lines established from human colorectal cancers. *Proc. Natl Acad. Sci. USA*, **94**, 10330–10334.

Jones,T.A., Zou,J.Y., Cowan,S.W. and Kjeldgaard,M. (1991) Improved methods for binding protein models in electron density maps and the location of errors in these models. *Acta Crystallogr. A*, **47**, 110–119.

Kishida,S., Yamamoto,H., Ikeda,S., Kishida,M., Sakamoto,I., Koyama,S. and Kikuchi,A. (1998) Axin, a negative regulator of the wnt signaling pathway, directly interacts with adenomatous polyposis coli and regulates the stabilization of β-catenin. *J. Biol. Chem.*, **273**, 10823–10826.

Kraulis,P.J. (1991) MOLSCRIPT—a program to produce both detailed and schematic plots of protein structures. *J. Appl. Crystallogr.*, **24**, 946–950.

Laskowski,R.A., MacArthur,M.W., Moss,D.S. and Thornton,J.M. (1993) PROCHECK—a program to check the stereochemical quality of protein structures. *J. Appl. Crystallogr.*, **26**, 283–291.

Mao,J., Yuan,H., Xie,W., Simon,M.I. and Wu,D. (1998) Specific involvement of G proteins in regulation of serum response factor-mediated gene transcription by different receptors. *J. Biol. Chem.*, **273**, 27118–27123.

McCartney,B.M., Dierick,H.A., Kirkpatrick,C., Moline,M.M., Baas,A., Peifer,M. and Bejsovec,A. (1999) *Drosophila* APC2 is a cytoskeletally-associated protein that regulates wingless signaling in the embryonic epidermis. *J. Cell Biol.*, **146**, 1303–1318.

Merritt,E.A. and Murphy,M.E.P. (1994) Raster3D version 2.0—a program for photorealistic molecular graphics. *Acta Crystallogr. D*, **50**, 869–873.

Miyoshi,Y. *et al*. (1992) Somatic mutations of the APC gene in colorectal tumors: mutation cluster region in the APC gene. *Hum. Mol. Genet.*, **1**, 229–233.

Miyoshi,Y., Iwao,K., Nagasawa,Y., Aihara,T., Sasaki,Y., Imaoka,S., Murata,M., Shimano,T. and Nakamura,Y. (1998) Activation of the β-catenin gene in primary hepatocellular carcinomas by somatic alterations involving exon 3. *Cancer Res.*, **58**, 2524–2527.

Morin,P.J., Sparks,A.B., Korinek,V., Barker,N., Clevers,H., Vogelstein,B. and Kinzler,K.W. (1997) Activation of β-catenin-Tcf signaling in colon cancer by mutations in β-catenin or APC. *Science*, **275**, 1787–1790.

Munemitsu,S., Albert,I., Souza,B., Rubinfeld,B. and Polakis,P. (1995) Regulation of intracellular β-catenin levels by the adenomatous polyposis coli (APC) tumor-suppressor protein. *Proc. Natl Acad. Sci. USA*, **92**, 3046–3050.

Navaza,J. (1994) AMoRe: an automated package for molecular replacement. *Acta Crystallogr. D*, **50**, 157–163.

Nicholls,A., Bharadwaj,R. and Honig,B. (1993) GRASP—graphical representation and analysis of surface properties. *Biophys. J.*, **64**, A116.

Orford,K., Crockett,C., Jensen,J.P., Weissman,A.M. and Byers,S.W. (1997) Serine phosphorylation-regulated ubiquitination and degradation of β-catenin. *J. Biol. Chem.*, **272**, 24735–24738.

Otwinowski,Z. and Minor,W. (1997) Processing of X-ray diffraction data collected in oscillation mode. *Methods Enzymol.*, **276**, 307–326.
Palacios,J. and Gamallo,C. (1998) Mutations in the β-catenin gene (CTNNB1) in endometrioid ovarian carcinomas. *Cancer Res.*, **58**, 1344–1347.
Pannu,N.S. and Read,R.J. (1996) Improved structure refinement through maximum likelihood. *Acta Crystallogr. A*, **52**, 659–668.
Polakis,P. (1999) The oncogenic activation of β-catenin. *Curr. Opin. Genet. Dev.*, **9**, 15–21.
Riese,J., Yu,X., Munnerlyn,A., Eresh,S., Hsu,S.C., Grosschedl,R. and Bienz,M. (1997) LEF-1, a nuclear factor coordinating signaling inputs from wingless and decapentaplegic. *Cell*, **88**, 777–787.
Rubinfeld,B., Albert,I., Porfiri,E., Fiol,C., Munemitsu,S. and Polakis,P. (1996) Binding of GSK3β to the APC–β-catenin complex and regulation of complex assembly. *Science*, **272**, 1023–1026.
Rubinfeld,B., Albert,I., Porfiri,E., Munemitsu,S. and Polakis,P. (1997a) Loss of β-catenin regulation by the APC tumor suppressor protein correlates with loss of structure due to common somatic mutations of the gene. *Cancer Res.*, **57**, 4624–4630.
Rubinfeld,B., Robbins,P., El-Gamil,M., Albert,I., Porfiri,E. and Polakis,P. (1997b) Stabilization of β-catenin by genetic defects in melanoma cell lines. *Science*, **275**, 1790–1792.
Sakanaka,C. and Williams,L.T. (1999) Functional domains of Axin. Importance of the C terminus as an oligomerization domain. *J. Biol. Chem.*, **274**, 14090–14093.
Sakanaka,C., Weiss,J.B. and Williams,L.T. (1998) Bridging of β-catenin and glycogen synthase kinase-3β by Axin and inhibition of β-catenin-mediated transcription. *Proc. Natl Acad. Sci. USA*, **95**, 3020–3023.
Satoh,S. *et al*. (2000) AXIN1 mutations in hepatocellular carcinomas, and growth suppression in cancer cells by virus-mediated transfer of AXIN1. *Nature Genet.*, **24**, 245–250.
Sheriff,S. and Hendrickson,W.A. (1987) Description of overall anisotropy in diffraction from macromolecular crystals. *Acta Crystallogr. A*, **43**, 118–121.
Shtutman,M., Zhurinsky,J., Simcha,I., Albanese,C., D'Amico,M., Pestell,R. and Ben-Ze'ev,A. (1999) The cyclin D1 gene is a target of the β-catenin/LEF-1 pathway. *Proc. Natl Acad. Sci. USA*, **96**, 5522–5527.
Smalley,M.J. *et al*. (1999) Interaction of Axin and Dvl-2 proteins regulates Dvl-2-stimulated TCF-dependent transcription. *EMBO J.*, **18**, 2823–2835.
Su,L.K., Vogelstein,B. and Kinzler,K.W. (1993) Association of the APC tumor suppressor protein with catenins. *Science*, **262**, 1734–1737.
Tesmer,J.J., Berman,D.M., Gilman,A.G. and Sprang,S.R. (1997) Structure of RGS4 bound to AlF4-activated G(iα1): stabilization of the transition state for GTP hydrolysis. *Cell*, **89**, 251–261.
Tetsu,O. and McCormick,F. (1999) β-catenin regulates expression of cyclin D1 in colon carcinoma cells. *Nature*, **398**, 422–426.
van de Wetering,M. *et al*. (1997) Armadillo coactivates transcription driven by the product of the *Drosophila* segment polarity gene dTCF. *Cell*, **88**, 789–799.
Willert,K. and Nusse,R. (1998) β-catenin: a key mediator of Wnt signaling. *Curr. Opin. Genet. Dev.*, **8**, 95–102.
Xu,L., Corcoran,R.B., Welsh,J.W., Pennica,D. and Levine,A.J. (2000) WISP-1 is a Wnt-1- and β-catenin-responsive oncogene. *Genes Dev.*, **14**, 585–595.
Yamamoto,H., Kishida,S., Uochi,T., Ikeda,S., Koyama,S., Asashima,M. and Kikuchi,A. (1998) Axil, a member of the Axin family, interacts with both glycogen synthase kinase 3β and β-catenin and inhibits axis formation of *Xenopus* embryos. *Mol. Cell. Biol.*, **18**, 2867–2875.
Yu,X., Waltzer,L. and Bienz,M. (1999) A new *Drosophila* APC homologue associated with adhesive zones of epithelial cells. *Nature Cell Biol.*, **1**, 144–151.
Zeng,L. *et al*. (1997) The mouse *fused* locus encodes Axin, an inhibitor of the Wnt signaling pathway that regulates embryonic axis formation. *Cell*, **90**, 181–192.
Zheng,B., De Vries,L. and Gist Farquhar,M. (1999) Divergence of RGS proteins: evidence for the existence of six mammalian RGS subfamilies. *Trends Biochem. Sci.*, **24**, 411–414.
Zurawel,R.H., Chiappa,S.A., Allen,C. and Raffel,C. (1998) Sporadic medulloblastomas contain oncogenic β-catenin mutations. *Cancer Res.*, **58**, 896–899.

Received December 3, 1999; revised and accepted March 20, 2000